Validity of ^{18}F-Fluorodeoxyglucose Imaging with a Dual-Head Coincidence Gamma Camera for Detection of Myocardial Viability

Shinji Hasegawa, Toshiisa Uehara, Hitoshi Yamaguchi, Kouichi Fujino, Hideo Kusuoka, Masatsugu Hori and Tsunehiko Nishimura

Division of Tracer Kinetics, Biomedical Research Center, and First Department of Medicine, Osaka University Medical School, Suita, Osaka, Japan

This study investigated the validity of myocardial ^{18}F-fluorodeoxy-glucose (FDG) imaging with a dual-head gamma camera operated in coincidence detection mode (DCD-I) by comparing this technique with conventional PET and SPECT with ultra-high-energy general-purpose collimators (UHGPs). **Methods:** The subjects included 5 healthy volunteers and 20 patients with a history of myocardial infarction. FDG (370 MBq) was injected intravenously after 75-g oral glucose loading, and PET, UHGP SPECT and DCD-I were performed 45, 60 and 210 min, respectively, after the injection. The target-to-background ratio of each imaging method was evaluated for the healthy volunteers by comparing myocardial uptake with uptake in the upper lungs or left ventricular cavity. Agreement between the results of the various imaging methods was investigated for the myocardial infarction patients, as was the validity of DCD-I for assessing myocardial viability as judged by comparison with myocardial perfusion SPECT. The left ventricular wall was divided into 18 regions, and uptake was evaluated using a five-grade defect score (0 = normal; 1–3 = low uptake; 4 = defect). **Results:** The mean ratio of myocardial counts to lung counts was lower on the DCD images (2.77 ± 1.12) than on the UHGP SPECT images (3.69 ± 0.98) ($P < 0.05$). In contrast, the mean ratio of myocardial counts to left ventricular cavity counts was higher on the DCD images (2.76 ± 1.36) than on the UHGP SPECT images (1.98 ± 0.70) ($P < 0.05$). For the patients, only 30.6% of the defect scores obtained by DCD-I agreed with the scores obtained by PET, and the defect scores in the inferior and septal walls were higher for the DCD images than for the PET images. When DCD-I was compared with PET without attenuation correction (AC), agreement improved to 58.3%. When corrected by a modified AC method, DCD-I improved to 48.1%. Agreement between UHGP SPECT and PET was 55.0%. Of the segments (64) for which the defect score of the myocardial perfusion image was greater than that for the FDG PET image, DCD-I without AC, DCD-I with AC and UHGP SPECT allowed an accurate diagnosis in 12 (18.8%), 31 (48.4%) and 43 (67.2%), respectively. **Conclusion:** The image quality of DCD-I is superior to that of UHGP SPECT. However, because the effect of attenuation is marked, accurate AC, by the transmission method, for example, is required to equal the validity of PET.

Identification of viable myocardium in the infarct area is important to achieving revascularization in myocardial infarction patients. ^{18}F-fluorodeoxyglucose (FDG) imaging by conventional PET has provided an accurate method of differentiating reversibly ischemic myocardium from irreversible scar tissue (*1,2*). However, clinical use of this technique is limited by the high cost of PET systems and cyclotron technology. Although myocardial viability has been assessed through myocardial perfusion images obtained with ^{201}Tl or ^{99m}Tc agents and SPECT, this method often underestimates viability (*3,4*).

Because of the relatively long physical half-life of ^{18}F, off-site production of FDG and subsequent transport to satellite laboratories have recently been proposed. As a result, myocardial FDG imaging with gamma cameras is anticipated, and a SPECT camera equipped with ultra-high-energy general-purpose collimators (UHGPs) has become available (*5–11*). Many studies have shown excellent image quality from FDG SPECT performed with UHGPs. However, when myocardial FDG uptake is low, images obtained with FDG SPECT are often of lower quality than are images obtained with PET. We therefore decided to validate myocardial FDG imaging with a dual-head gamma camera operated in coincidence detection mode (DCD imaging, or DCD-I), which was expected to provide better image quality than does UHGP SPECT (*12–16*).

MATERIALS AND METHODS

Myocardial infarction patients, healthy volunteers and a myocardial phantom with defects were examined with DCD-I, UHGP SPECT and PET. The severity of the defects, target-to-background ratio and agreement between the results obtained by these FDG techniques were assessed with and without attenuation. The myocardial infarction patients were also examined with ^{99m}Tc-

tetrofosmin (TF) perfusion SPECT. Discordance between the severity of defects seen on the TF SPECT and FDG images was used as a marker of hypoperfused but viable myocardium. The sensitivity and specificity of DCD-I and UHGP SPECT for viability measurement were assessed by comparison with those of PET, the gold standard.

Phantom Study

A myocardial phantom having three transmural defects, 1-cm diameter each, in the lateral wall, inferior wall and septal wall was used to investigate the ability of each technique to depict defects in myocardial FDG uptake. The phantom represented a torso, and the mediastinum and lungs were filled with air and cork, respectively. The space corresponding to the myocardium was filled with 18.5 kBq/mL FDG. Images were acquired with DCD-I, UHGP SPECT and PET. Attenuation on PET images was corrected using the transmission method; attenuation on DCD and UHGP SPECT images was not corrected. Square regions of interest ([ROIs] 4 × 4 pixels) were set on the defect and in its vicinity on the lateral, inferior and septal walls, and the ratio of the defect count to the count in the vicinity was determined.

Subjects

The subjects were 5 healthy male volunteers and 20 patients (18 men, 2 women; mean age 64.1 ± 9.1 y) with a history of myocardial infarction more than 1 mo previously. Wall motion was assessed by echocardiography in all subjects, and the left ventricular ejection fraction was measured by the Teichholz method (17). The study was approved by the ethics committee of Osaka University Hospital, and all healthy volunteers and patients gave informed consent.

Fluorodeoxyglucose Imaging

Figure 1 shows the study protocol. PET was performed with a whole-body camera (SET-2400W [Headtome V]; Shimadzu Medico Co., Kyoto, Japan). The specifications were 63 contiguous transaxial slices 3.125 mm apart; in-plane and axial resolutions of 3.7 and 5 mm, respectively, full width at half maximum (FWHM); and a sensitivity of 440 cpm/MBq/mL. A 75-gm dose of glucose was orally administered 50 min before intravenous injection of FDG. After positioning, transmission scanning for attenuation correction (AC) was performed for 10 min with rotating ⁶⁷Ge line sources. Then, 370 MBq FDG were injected intravenously, and data acquisition was started 45 min after the injection. Transaxial tomographic FDG PET images (128 × 128 matrices) were reconstructed from the emission data acquired over 10 min by filtered backprojection using a ramp filter and a Butterworth convolution filter. The images, with AC by transmission data or without AC, were resliced into a series of short-axis and vertical long-axis images.

The subjects underwent two additional FDG imaging modes

with a gamma camera (Vertex Plus MCD; ADAC Laboratories, Milpitas, CA). One was performed using the SPECT mode and an L-type dual-head detector equipped with UHGPs for 511 keV, and the other was performed using DCD and a parallel dual-head detector without UHGPs. UHGP SPECT was performed in 32 (16 × 2) steps over 180° (90 × 2) just after the PET acquisition (50 s per step). DCD-I was performed in 32 steps over 360° (180 × 2) 210 min after FDG injection (50 s per step), when the counts in the field of view were reduced. DCD-I is not capable of operating as great a number of counts as conventional PET. Workers at Osaka University Medical School confirmed that when more than 1000 kcps (single photons) are in the field of view, the counts are saturated and the images incorrect and that when 500–1000 kcps (single photons) are in the field of view, the images are suitable (unpublished data). The data were reconstructed by backprojection into transaxial slices with a Butterworth filter (UHGP SPECT: 0.5 cycle/mm cutoff, order of 5.0; DCD-I: 0.45 cycle/mm cutoff, order of 8.0) and resliced into a series of short-axis and vertical long-axis images. With UHGP SPECT, in-plane resolution was 9.2 mm FWHM with 64 × 64 matrices, and sensitivity was 15 cpm/MBq/mL. With DCD-I, in-plane resolution was 4.8 mm FWHM with 128 × 128 matrices, and sensitivity was 160 cpm/MBq/mL. The DCD-I data were also reconstructed with a modification of the AC of Chang (18,19), in which the adsorption rate was considered to be homogeneous throughout the body. Each projection pixel was multiplied by a factor that was based on the attenuation coefficient of 511 keV in water (0.095) and the length of the coincidence path.

Myocardial Perfusion SPECT

Myocardial perfusion SPECT with ⁹⁹ᵐTc-TF (Nihon Mediphysics, Hyogo, Japan) was performed within 2 wk of the FDG study on all patients who had a history of myocardial infarction. ⁹⁹ᵐTc-TF (370 MBq) was injected intravenously with the patient at rest, and the images were obtained 30–60 min after the injection with a three-head rotating gamma camera (GCA9300A/HG; Toshiba Medico Co., Tokyo, Japan) equipped with UHGPs centered on the 141-KeV photopeak. Each image was reconstructed from projection data acquired over a 360° elliptical orbit around each patient's thorax, in 3° increments, for 60 s.

Data Analysis

The image data from the healthy volunteers were analyzed to find the target-to-background ratio of each imaging method. Square ROIs (4 × 4 pixels) were set on the upper lung, the left ventricular cavity and the left ventricular myocardium (anterior, lateral, inferior and septal walls, Fig. 2) at the midventricular level of the short-axis image. The ratios of the myocardial counts to the lung counts and of the myocardial counts to the left ventricular cavity counts were determined as indicators of the target-to-background ratio.
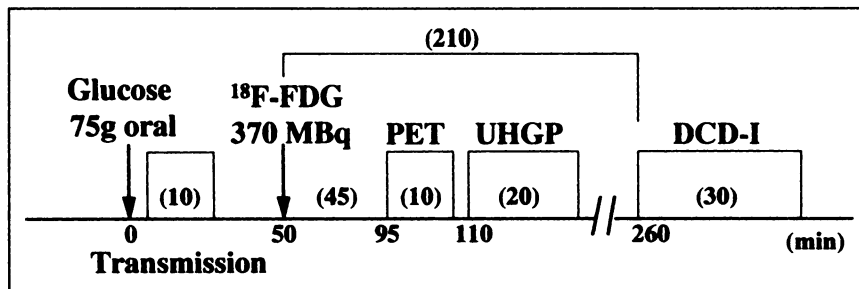

FIGURE 1. ¹⁸F-fluorodeoxyglucose (FDG) imaging protocol. FDG (370 MBq) was injected intravenously after 75-g oral glucose loading, and conventional PET, SPECT with ultra-high-energy general-purpose collimators (UHGPs) and imaging with dual-head gamma camera operated in coincidence detection mode (DCD-I) were performed 45, 60 and 210 min, respectively, after injection.
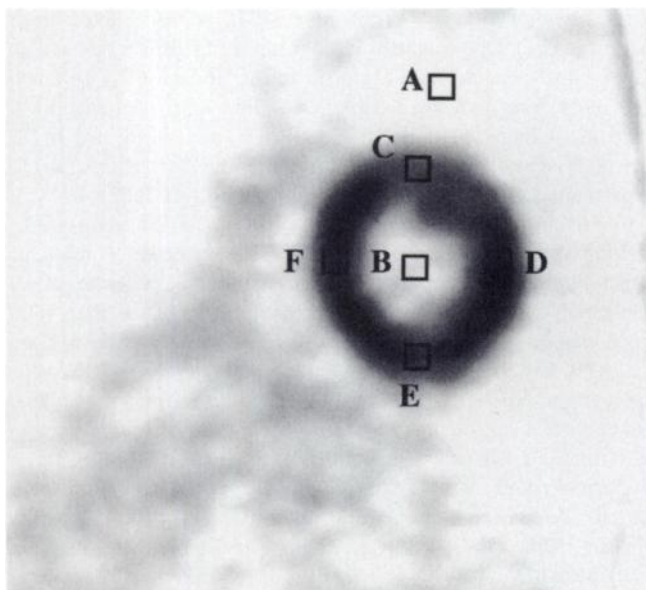
FIGURE 2. ROIs for target-to-background ratio in healthy volunteers. Square ROIs (4 × 4 pixels) were set on upper lung (A); left ventricular cavity (B); and anterior (C), lateral (D), inferior (E) and septal (F) walls of left ventricle.

The SPECT or PET images of the patients were divided into 18 segments for further analysis (Fig. 3). The short-axis images at the midventricular level and low-ventricular level were divided into 8 segments each (4 anterior, 4 septal, 4 inferior and 4 lateral), and the apex on the midvertical long-axis image was divided into 2 segments. Segmental defects of FDG or TF uptake were independently scored visually by two experienced, masked observers using a five-point system (0 = normal; 1 = mildly decreased uptake; 2 = moderately decreased uptake; 3 = severely decreased uptake; 4 = defect). Whenever the two observers' scores differed, a third independent observer adjusted the score. The inter- and intraindividual reproducibility of this analysis was 80.2% and 87.2%, respectively. When a segment had a defect score that was higher for the perfusion image than for the FDG image, that segment was defined as one for which the perfusion image underestimated the amount of viable myocardium (20).

In addition, polar maps were made from the short-axis heart images and divided into 24 segments (8 segments each in the apical, middle and basal portions). Regional percentage uptake of FDG in the segments on the polar map was measured using PET with and without AC, DCD-I with and without the modified AC of
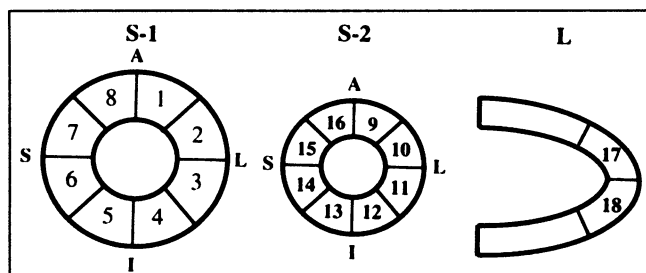

FIGURE 3. Eighteen segments used for myocardial infarction study. A = anterior; I = inferior; large L = midvertical long-axis image; small L = lateral; S = septal; S-1 = short-axis image at midventricle level; S-2 = short-axis image at low-ventricle level.

Chang (18,19) and UHGP SPECT, and the results of these techniques were correlated.

Statistical Analysis

Data are presented as mean ± SD. A paired Student t test was used for statistical testing. Correlations were assessed by the Pearson correlation coefficient and Fisher test, and agreement was assessed by Bland-Altman plotting. Results for which P was <0.05 were considered statistically significant.

RESULTS

Phantom Study

Figure 4 shows the images of the myocardial phantom with defects in the lateral, inferior and septal wall obtained using PET with AC, DCD-I without AC and UHGP SPECT. The DCD images were as sharp as the PET images. However, the images of the inferoseptal wall obtained using DCD-I were attenuated, and the defects in the inferior wall and the septum were unclear. In addition, the shape of the inferior wall in the DCD image seemed flat because of attenuation. Anteroposterior dimensions of lung cancer tumors have been reported to be significantly larger on FDG PET scans without AC than on FDG PET scans with AC (21). The same phenomenon may make the septum and lateral walls appear longer and the inferior wall appear flat. In contrast, images obtained using UHGP SPECT are not sharp and are more affected by a partial-volume effect. Figure 5 shows the count ratio of the defect to the vicinity of the phantom. The ratio on UHGP SPECT was nearly 1, making differentiation of the defect difficult. However, UHGP SPECT was not influenced by the attenuation.
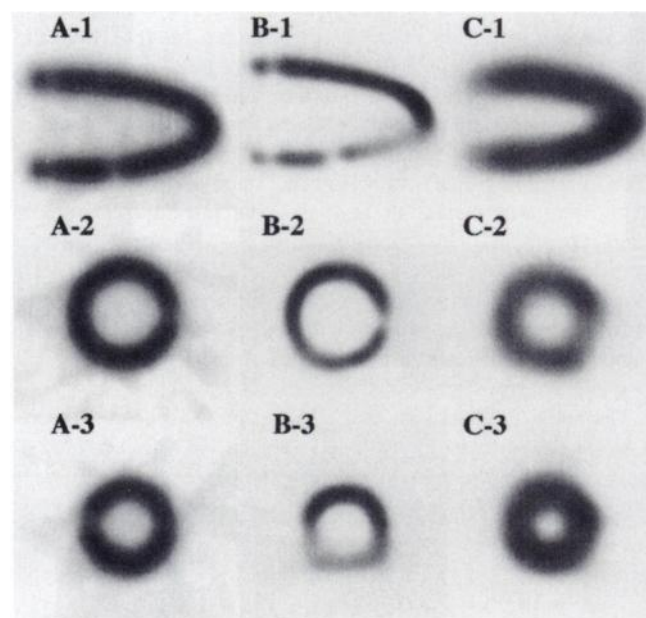

FIGURE 4. Images of myocardial phantom with defects in lateral, inferior and septal walls obtained using PET with AC (A), DCD-I without AC (B) and UHGP SPECT (C). 1 = vertical long-axis image; 2 = basal short-axis image; 3 = apical short-axis image.
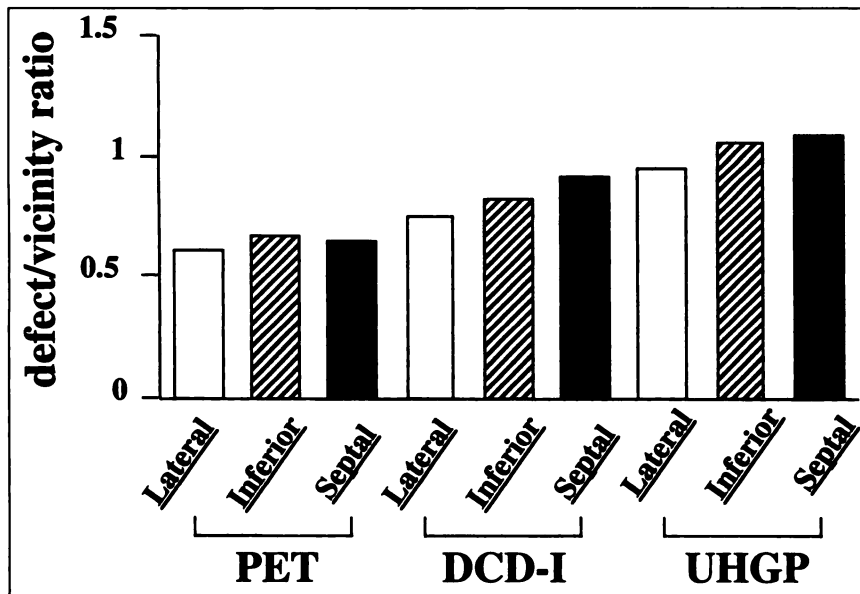
FIGURE 5. Ratio of defect counts to vicinity counts of phantom on PET, coincidence detection mode imaging (DCD-I) and ultra-high-energy general-purpose collimator (UHGP) SPECT. White bar = lateral wall; shaded bar = inferior wall; black bar = septal wall.

Control Study

Table 1 summarizes the ratios of myocardial counts to lung counts or left ventricular cavity counts for the healthy volunteers. Both ratios were higher for the PET images than for the DCD or UHGP SPECT images ($P < 0.05$). The ratio of myocardial counts to lung counts was lower ($P < 0.05$) for the DCD images (2.77 ± 1.12) than for the UHGP SPECT images (3.69 ± 0.98). In contrast, the ratio of myocardial counts to left ventricular cavity counts was higher ($P < 0.05$) for the DCD images (2.76 ± 1.36) than for the UHGP SPECT images (1.98 ± 0.70). These results suggest that the background count of the DCD images was as high as that of the UHGP SPECT images but that the effect of scatter from the myocardium to the surrounding area was less and the borderline was clearer.

Myocardial Infarction Study

Imaging was performed more than 1 mo after the onset of myocardial infarction for all patients. In 4 patients the

TABLE 1
Mean Ratios (±SD) of Myocardial Counts to Lung Counts and Left Ventricular Cavity Counts

Type of count	PET with AC	DCD-I without AC	UHGP SPECT without AC
Myocardium to lung	44.15 ± 14.87*	2.77 ± 1.12†	3.69 ± 0.98
Myocardium to left ventricular cavity	7.04 ± 2.14*	2.76 ± 1.36†	1.98 ± 0.70

*$P < 0.05$ vs DCD-I and UHGP SPECT.
†$P < 0.05$ vs UHGP SPECT.
AC = attenuation correction; DCD-I = coincidence detection mode imaging; UHGP = ultra-high-energy general-purpose collimator.

infarction was in the region of the left anterior descending artery (LAD): in the region of the first diagonal branch in 1, the left circumflex artery (LCX) in 2, the right coronary artery (RCA) in 5, the LAD and RCA in 3, the LAD and LCX in 3 and all three vessels in 2. Four patients had one-vessel disease; 4, two-vessel disease; and 12, three-vessel disease. The left ventricular ejection fraction was less than 40% in 7 of the 20 patients. Thirty vessels were infarcted: 10 Q wave and 20 non–Q wave. Diabetes mellitus had been diagnosed in 11 of the 20 patients.

In 3 patients (15%), the UHGP SPECT images were of poor quality and the DCD images had a lower background count than did the UHGP SPECT images. Two of these 3 patients had diabetes mellitus, and 1 of these 2 and the third had poor left ventricular function with three-vessel infarction. Good-quality images were acquired for the other patients.

According to the scoring assessment, the defect scores obtained using DCD-I without AC agreed well with those obtained using PET for 110 (30.6%) of the 360 regions (Table 2). The defect scores in the inferior and septal walls were higher for the DCD images than for the PET images (Fig. 6A). Because the suspicion was that this difference was mainly caused by the attenuation of DCD-I, DCD-I without AC was compared with PET without AC (Table 3). The results showed that when AC was not performed for PET, the difference between the inferior and the septal walls was reduced (Fig. 6B) and agreement improved to 58.3% (210 regions). When DCD-I was corrected by the modified AC of Chang (18,19), agreement with PET with AC improved to 48.1% (173 regions, Table 4, Fig. 6C). This method was not sufficient, because the apex or inferior wall was sometimes attenuated because of improper correction. However, the defect score of UHGP SPECT agreed well with that of PET with AC in 198 (55.0%) of 360 regions (Table 5), and the

TABLE 2
Relationship Between DCD-I and PET

Defect scores in PET with AC	Defect scores in DCD-I without AC				
	0	1	2	3	4
0	55	25	43	21	4
1	21	12	26	14	2
2	20	10	15	21	13
3	1	7	6	18	9
4	0	0	3	4	10

DCD-I = coincidence detection mode imaging; AC = attenuation correction.
Agreement rate is 30.6%.

TABLE 3
Relationship Between DCD-I Without AC and PET Without AC

Defect scores in PET without AC	Defect scores in DCD-I without AC				
	0	1	2	3	4
0	89	22	5	2	1
1	5	16	22	9	2
2	2	14	60	38	7
3	1	2	6	26	9
4	0	0	0	3	19

DCD-I = coincidence detection mode imaging; AC = attenuation correction.
Agreement rate is 58.3%.

defect score in the lateral wall and apex tended to be higher than in the other regions (Fig. 6D). UHGP SPECT may agree better with PET because the effect of scatter and the effect of attenuation cancel out each other.

Figure 7 shows the relationship between regional FDG uptake obtained by polar map analysis by PET and by gamma camera imaging. Regional percentage uptake of FDG found using PET correlated significantly with that found using gamma camera imaging, and the agreement was confirmed with Bland-Altman plotting. The correlation was weaker between PET and DCD-I without AC ($r = 0.162$, $P = 0.001$) than between PET and UHGP SPECT ($r = 0.395$, $P < 0.0001$). However, the correlation between PET and DCD-I with the modified AC of Chang (18,19) ($r = 0.452$, $P < 0.0001$) was better than the correlation between PET and UHGP SPECT. The correlation between PET without AC and DCD-I without AC was the best of all ($r = 0.807$, $P < 0.0001$). These results indicate that PET agrees with DCD-I with AC as well as with UHGP SPECT. PET

appears to agree with DCD-I better than with UHGP SPECT when the AC of DCD-I is more accurate.

Accuracy in diagnosing myocardial viability using DCD-I and UHGP SPECT was assessed. For 64 segments, the defect score for the myocardial perfusion image was greater than that for the FDG PET image. DCD-I without AC, DCD-I with AC and UHGP SPECT permitted accurate diagnosis in 12 (18.8%), 31 (48.4%) and 43 (67.2%) segments, respectively. Of 30 infarcted vessel regions, TF led to underestimation of viable myocardium in 22 regions for which viability was accurately measured with PET, whereas DCD-I without AC, DCD-I with AC and UHGP SPECT led to accurate diagnosis in 15 (68.2%), 8 (36.4%) and 21 (95.5%) regions, respectively. Table 6 summarizes the diagnostic accuracy of DCD-I with or without AC and UHGP SPECT for myocardial viability, with the findings of PET considered the gold standard. Although the sensitivity of DCD-I with AC was higher than that of DCD-I without
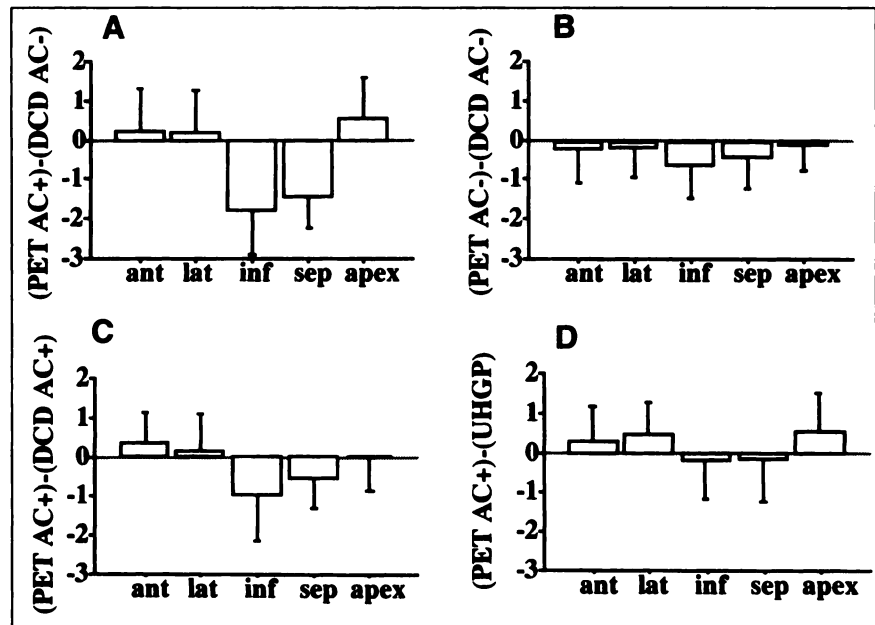

FIGURE 6. Regional differences in defect score between PET, coincidence detection mode imaging (DCD-I) and ultra-high-energy general-purpose collimator (UHGP) SPECT. (A) PET with attenuation correction (AC+) and DCD-I without attenuation correction (AC−). (B) PET without AC and DCD-I without AC. (C) PET with AC and DCD-I with modified AC of Chang (18,19). (D) PET with AC and UHGP SPECT.

TABLE 4
Relationship Between DCD-I with AC and PET

Defect scores in PET with AC	Defect scores in DCD-I with AC				
	0	1	2	3	4
0	79	39	20	8	2
1	16	35	19	5	0
2	15	14	24	25	1
3	1	2	7	26	5
4	0	0	0	8	9

DCD-I = coincidence detection mode imaging; AC = attenuation correction.
Agreement rate is 48.1%.

AC, the sensitivity of UHGP SPECT was higher than that of either DCD-I with AC or DCD-I without AC. DCD-I with AC had the best specificity and positive predictive value of the three imaging methods, but little difference was seen between DCD-I and UHGP SPECT. These results suggest that the image quality of DCD-I is superior to that of UHGP SPECT but that UHGP SPECT allows more accurate diagnosis than does DCD-I performed without the more accurate AC.

Echocardiography revealed akinesis, hypokinesis and normokinesis in 16, 40 and 8 segments, respectively, of the 64. Presumably, the segments that showed normokinesis were affected by attenuation artifacts in the TF images. The sensitivity of all techniques, especially UHGP SPECT, was better for akinetic segments than for hypokinetic or normokinetic segments (Table 7).

In the 3 of 20 patients treated with percutaneous transluminal coronary angioplasty, recovery of wall motion could not be assessed because of restenosis. Twelve patients underwent coronary artery–aorta bypass grafting after the FDG study. One died after the operation, but the other 11 were followed up for 3–6 mo postoperatively. The other 5 patients did not undergo revascularization. The defect score on the myocardial perfusion images was 3 or 4 for 22 of the 198 segments. Because wall motion improved in 12 of these 22

TABLE 5
Relationship Between UHGP SPECT and PET

Defect scores in PET with AC	Defect scores in UHGP SPECT				
	0	1	2	3	4
0	114	27	5	1	1
1	28	33	12	0	2
2	21	23	25	9	1
3	4	7	13	12	5
4	0	0	1	2	14

UHGP = ultra-high-energy general-purpose collimator; AC = attenuation correction.
Agreement rate is 55.0%.

segments, their myocardium was viable. PET allowed diagnosis of viability in 7 of the 12 segments (58.3%). DCD-I without AC, DCD-I with the modified AC of Chang (18,19) and UHGP SPECT permitted diagnosis in 5 (41.7%), 5 (41.7%) and 7 (58.3%) segments, respectively, of these 12.

Figures 8 and 9 show a patient with a history of anterior and posterolateral myocardial infarction. In this patient, the modified AC of Chang (18,19) revealed the apexlike defect in the DCD image, and UHGP SPECT failed to detect the small defect in the inferior wall.

DISCUSSION
Spatial Resolution

Image quality and spatial resolution are critical to assessing regional viability in patients with low FDG uptake caused by infarction or diabetes mellitus. We evaluated the image quality and spatial resolution of DCD-I in comparison with PET and UHGP SPECT using a myocardial phantom with three defined defects. The spatial resolution of DCD-I was superior to that of UHGP SPECT and was only slightly poorer than that of PET. One-centimeter defects on the myocardial phantom could be differentiated by DCD-I but not by UHGP SPECT. This finding is attributable not only to the superiority of the intrinsic resolution of DCD-I but also to its ability to image with 128 × 128 matrices, the same as for PET but impossible for UHGP SPECT (64 ×64 matrices) because of poor sensitivity. However, the effect of attenuation on DCD-I was marked, so that detection of small defects on the inferoseptal wall was poor.

Scatter Effect and Image Quality

The scatter effect was evaluated in the healthy volunteers. With DCD-I, most of the Compton scatter is cut by coincidence detection, whereas UHGP SPECT images are markedly affected by Compton scatter. In DCD-I, however, the gamma rays that strike obliquely because of imperfect collimation are not cut, just as they are not cut in three-dimensional PET (22,23). These rays increase the random coincidence counts, but in UHGP SPECT a greater number of oblique rays are cut by the collimator. Our study showed that the myocardium-to-lung count ratio was slightly lower with DCD-I than with UHGP SPECT and that the myocardium-to-left ventricle count ratio was higher with DCD-I than with UHGP SPECT. These results suggest that the image of the upper lung is affected by the oblique rays that have broad distribution and that the image of the ventricular cavity is markedly affected by Compton scatter from the myocardium. Because of the increased number of scattered photons near the myocardium and the poor spatial resolution, the boundary is unclear, resulting in deterioration of UHGP SPECT image quality. In two-dimensional PET, most of the oblique rays are cut by the septa, and the most of the Compton scatter is cut by coincidence detection. Thus, the scatter effect is low. The image quality of PET is therefore superior to that of the other two imaging techniques.
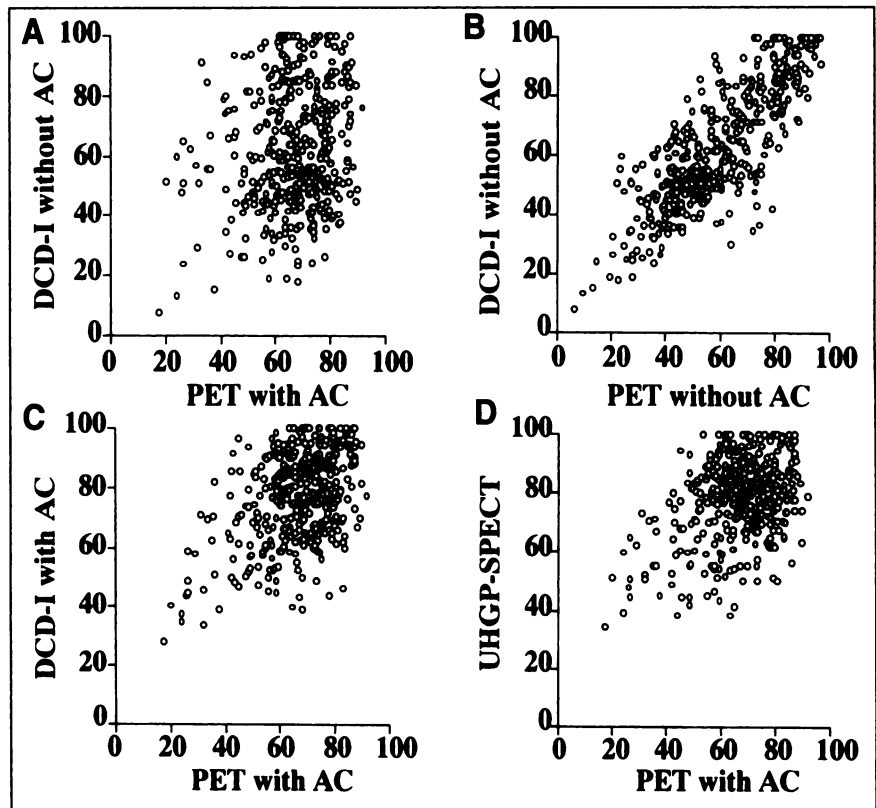
FIGURE 7. Relationship between regional percentage uptake of FDG by PET and coincidence detection mode imaging (DCD-I) and ultra-high-energy general-purpose collimator (UHGP) SPECT. (A) PET and DCD-I without attenuation correction (AC) (r = 0.162). (B) PET without AC and DCD-I without AC (r = 0.807). (C) PET and DCD-I with modified AC of Chang (18,19) (r = 0.452). (D) PET and UHGP SPECT (r = 0.395).

Assessment of Myocardial Viability

This study made clear the validity of DCD-I and UHGP SPECT in the assessment of myocardial viability and their degree of agreement with PET. DCD-I without AC was inferior to UHGP SPECT in agreement with PET and in sensitivity for detecting viable myocardium, but DCD-I was almost equal to UHGP SPECT in specificity. When the modified AC of Chang (18,19) was performed, both agreement with PET and sensitivity for detecting viability improved, but DCD-I was still inferior to UHGP SPECT in sensitivity. DCD-I with AC was superior to UHGP SPECT in specificity and positive predictive value. In UHGP SPECT, the effect of scatter and the effect of attenuation cancel out each other (24). In contrast, in DCD-I, the attenuation effect is stronger than the scatter effect, and

attenuation becomes a major problem. The modified AC of Chang (18,19) used in this study is inadequate for clinical application because the method is not compatible with variety in patients. The chest is not homogeneous. The method is intended for uniform correction and is optimal for the brain, not the chest. However, agreement was better between DCD-I without AC and conventional PET without AC than between UHGP SPECT and conventional PET with AC, and correlation of FDG uptake calculated by polar map analysis was good between the two techniques. Thus, DCD-I may provide a useful approach if more accurate AC, such as the transmission method, becomes available.

On a segment basis, agreement between PET and gamma camera imaging was poorer than in previous studies (6–8,10,11). Those studies showed good agreement (76%–94%) between PET and UHGP SPECT, but this study showed only

TABLE 6
Comparison of Assessments of Myocardial Viability by DCD-I and UHGP SPECT

Index	DCD-I with AC (%)	DCD-I without AC (%)	UHGP-SPECT (%)
Sensitivity	48.4	18.8	67.2
Specificity	94.6	92.6	91.6
Positive predictive value	66.0	35.3	63.2
Negative predictive value	89.5	84.1	92.8

DCD-I = coincidence detection mode imaging; UHGP = ultra-high-energy general-purpose collimator; AC = attenuation correction.

TABLE 7
Wall Motion and Sensitivity of DCD-I and UHGP SPECT

Type of wall motion	No. of segments	DCD-I with AC (%)	DCD-I without AC (%)	UHGP SPECT (%)
Akinesis	16	56.3	31.3	93.8
Hypokinesis	40	50.0	17.5	57.5
Normokinesis	8	25.0	0.0	62.5

DCD-I = coincidence detection mode imaging; UHGP = ultra-high-energy general-purpose collimator; AC = attenuation correction.
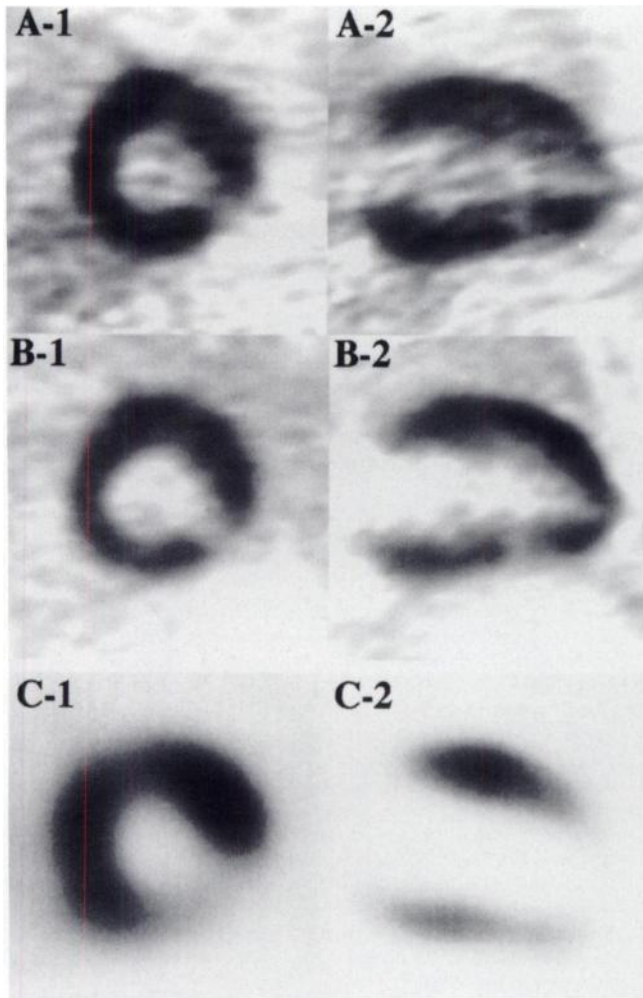
FIGURE 8. (A) FDG PET images show residual myocardium in anteroapical wall and posterolateral wall. (B) Images obtained without AC by transmission scan show marked decrease in intensity in inferior wall. (C) ^{99m}Tc-TF SPECT images show that residual myocardium seen in A appears nonviable. 1 = short-axis images; 2 = vertical long-axis images.

techniques and wall motion was investigated. The validity of UHGP SPECT was good in the segments showing akinesis (Table 7). UHGP SPECT also allowed viability to be diagnosed as accurately as did PET in the segments that the myocardial perfusion images showed to be poorly viable, and UHGP SPECT showed functional improvement after revascularization. These results suggest that UHGP SPECT is good for detecting slightly viable segments.

Counting Rate Capability

DCD-I is inferior to PET in capability of operating high counts. In this study, that problem was solved by delaying the acquisition to 210 min after the injection of 370 MBq FDG. However, if acquisition begins at the same time as PET, reduction of the FDG dose to approximately 185 MBq might maintain image quality because of the high sensitivity of DCD-I. However, the low sensitivity of UHGP SPECT
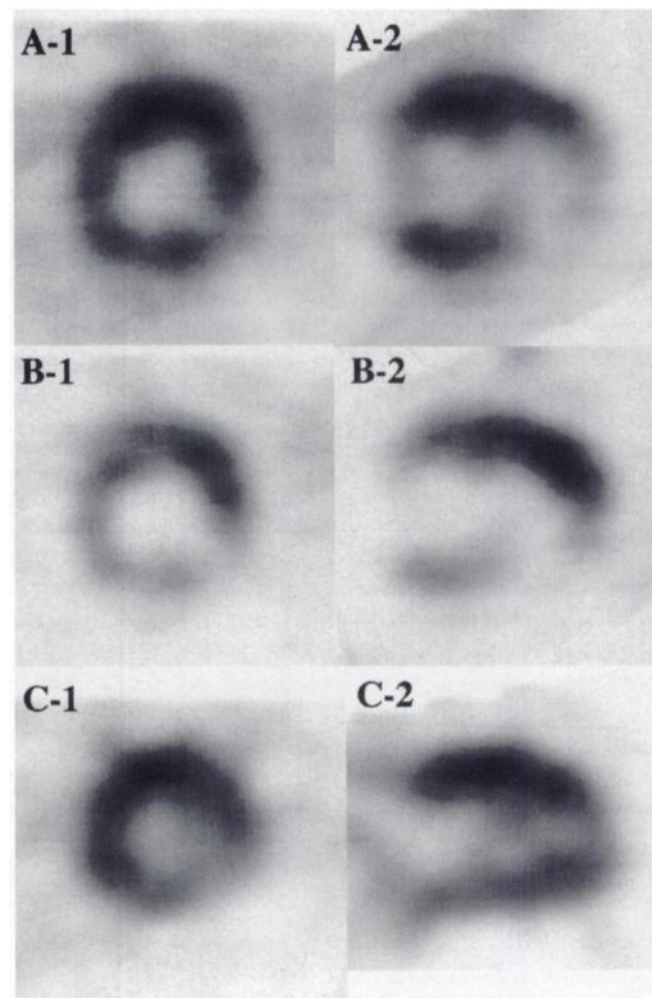

FIGURE 9. DCD images with (A) and without (B) modified AC of Chang (17,18) and UHGP SPECT images (C) of same patient as in Figure 8. Both imaging methods identified viable myocardium in anteroapical and posterolateral walls, but DCD images, especially without AC, were affected by attenuation. A-2 shows apexlike defect made apparent by AC of Chang (17,18). C-2 shows that UHGP SPECT failed to detect small defect in inferior wall. 1 = short-axis images; 2 = vertical long-axis images.

55.0% agreement. In addition, the sensitivity of UHGP SPECT for myocardial viability on a segment basis was lower than in other studies (Chen et al. [10]: 86%, Srinivasan et al. [11]: 88%). In previous studies, myocardial viability was evaluated as either present or absent. By contrast, in this study the extent of FDG uptake was judged using a five-grade defect score, and the number of segments in which uptake was analyzed—18—was more than in previous studies. These differences may have caused the poorer agreement. In fact, UHGP SPECT showed good sensitivity in assessments based on an infarcted vessel region (95.5%).

In clinical situations, assessment of viability is important in segments with severely abnormal wall motion. However, assessment of the amount of viable myocardium is also important in determining prognosis. Therefore, some segments were included that showed obvious viability on perfusion SPECT images or wall motion in the assessment, and the relationship between viability evaluated by these

indicates that imaging with such a small dose would be impossible. These findings suggest that off-site production of FDG and subsequent transport to satellite laboratories would be advantageous for DCD-I.

Limitations

The examinations were performed after oral glucose loading—a method insufficient for assessing myocardial viability. The quality of the FDG images may be poor because of low myocardial uptake and a high background count, particularly in diabetic patients (25,26). The insulin-clamp method may be necessary. In fact, the images of diabetic patients tended to be poor, and the diagnostic sensitivity of gamma camera imaging for myocardial viability was poor (DCD-I with AC: 36.1%, DCD-I without AC: 11.1%, UHGP SPECT: 50.0%). Two of the 3 patients whose UHGP SPECT images were of poor quality had diabetes. However, in this study population, viability could be judged for all FDG PET images after oral glucose loading. The main purpose of the study was to compare gamma camera FDG imaging with FDG PET, and complications such as diabetes did not interfere with the results.

In this study, PET, DCD-I and UHGP SPECT acquisitions were started at different intervals after the FDG injection. The different intervals may be responsible for the differences in distribution in the myocardium or other organs and the blood. Enhanced uptake in hibernating regions 24 h after injection has been reported for ^{201}Tl myocardial SPECT images (27), and similar changes in FDG uptake may occur in hibernating regions. Therefore, delayed acquisition may be advantageous in detecting myocardial viability with DCD-I.

CONCLUSION

Imaging of myocardial FDG uptake with a dual-head gamma camera operated in DCD is superior in spatial resolution, count sensitivity and quality to imaging with a SPECT camera equipped with UHGPs. However, because the effect of attenuation is marked, accurate AC, such as by the transmission method, is necessary to obtain results equivalent to those of PET.

ACKNOWLEDGMENTS

REFERENCES

1. Tillisch J, Brunken R, Marshall R, et al. Reversibility of cardiac wall-motion abnormalities predicted by positron tomography. N Engl J Med. 1986;314:884–888.
2. Tamaki N, Kawamoto M, Tadamura E, et al. Prediction of reversible ischemia after revascularization: perfusion and metabolic studies with positron emission tomography. Circulation. 1995;91:1697–1705.
3. Maddahi J, Schelbert H, Brunken R, Di Carli M. Role of thallium-201 and PET imaging in evaluation of myocardial viability and management of patients with coronary artery disease and left ventricular dysfunction. J Nucl Med. 1994;35:707–715.
4. vom Dahl J, Altehoefer C, Sheehan FH, et al. Effect of myocardial viability

5. Bax JJ, Visser FC, van Lingen A, et al. Feasibility of assessing regional myocardial uptake of ^{18}F-fluorodeoxyglucose using single photon emission computed tomography. Eur Heart J. 1993;14:1675–1682.
6. Martin WH, Delbeke D, Patton JA, et al. FDG SPECT: correlation with FDG PET. J Nucl Med. 1995;36:988–995.
7. Burt RW, Perkins OW, Oppenheim BE, et al. Direct comparison of fluorine-18-FDG SPECT, fluorine-18-FDG PET and rest thallium-201 SPECT for detection of myocardial viability. J Nucl Med. 1995;36:176–179.
8. Bax JJ, Visser FC, Blanksma PK, et al. Comparison of myocardial uptake of fluorine-18-fluorodeoxyglucose imaged with PET and SPECT in dyssynergic myocardium. J Nucl Med. 1996;37:1631–1636.
9. Bax JJ, Cornel JH, Visser FC, et al. Prediction of recovery of myocardial dysfunction after revascularization. Comparison of fluorine-18 fluorodeoxyglucose/thallium-201 SPECT, thallium-201 stress-reinjection SPECT and dobutamine echocardiography. J Am Coll Cardiol. 1996;28:558–564.
10. Chen EQ, MacIntyre WJ, Go RT, et al. Myocardial viability studies using fluorine-18-FDG SPECT: a comparison with fluorine-18-FDG PET. J Nucl Med. 1997;38:582–586.
11. Srinivasan G, Kitsiou AN, Bacharach SL, Bartlett ML, Miller-Davis C, Dilsizian V. [^{18}F]fluorodeoxyglucose single photon emission computed tomography: can it replace PET and thallium SPECT for the assessment of myocardial viability? Circulation. 1998;97:843–850.
12. Shreve PD, Steventon RS, Deters EC, Kison PV, Gross MD, Wahl RL. Oncologic diagnosis with 2-[fluorine-18]fluoro-2-deoxy-D-glucose imaging: dual-head coincidence gamma camera versus positron emission tomographic scanner. Radiology. 1998;207:431–437.
13. Abdel Dayem HM, Radin AI, Luo JQ, et al. Fluorine-18-fluorodeoxyglucose dual-head gamma camera coincidence imaging of recurrent colorectal carcinoma. J Nucl Med. 1998;39:654–656.
14. Stokkel MP, Terhaard CH, Mertens IJ, Hordijk GJ, van Rijk PP. Fluorine-18-FDG detection of laryngeal cancer postradiotherapy using dual-head coincidence imaging. J Nucl Med. 1998;39:1385–1387.
15. Abu Judeh HH, Singh M, Masdeu JC, Abdel Dayem HM. Discordance between FDG uptake and technetium-99m-HMPAO brain perfusion in acute traumatic brain injury. J Nucl Med. 1998;39:1357–1359.
16. Sandler MP, Bax JJ, Patton JA, Visser FC, Martin WH, Wijns W. Fluorine-18-fluorodeoxyglucose cardiac imaging using a modified scintillation camera. J Nucl Med. 1998;39:2035–2043.
17. Teichholz LE, Krulen T, Herman MV, Gorlin R. Problems in echocardiographic angiographic correlations in the presence or absence of asynergy. Am J Cardiol. 1976;37:7–11.
18. Chang LT. A method for attenuation correction in radionuclide computed tomography. IEEE Trans Nucl Sci. 1978;26:638–643.
19. Gullberg GT, Budinger TF. The use of filtering methods to compensate for constant attenuation in single-photon emission computed tomography. IEEE Tran Biomed Eng. 1981;28:142–157.
20. Machac J, Dangas G, Pandit N, et al. Prediction of left ventricular functional recovery after elective early post infarction revascularization by MIBI/FDG SPECT imaging and dobutamine echocardiography [abstract]. J Nucl Med. 1998;39(suppl):18P.
21. Zasadny KR, Kison PV, Quint LE, Wahl RL. Untreated lung cancer: quantification of systematic distortion of tumor size and shape on non-attenuation-corrected 2-[fluorine-18]fluoro-2-deoxy-D-glucose PET scans. Radiology. 1996;201:873–876.
22. Townsend DW, Wensveen M, Byars LG, et al. A rotating PET scanner using BGO block detectors: design, performance and applications. J Nucl Med. 1993;34:1367–1376.
23. Budinger TF, Brennan KM, Moses WW, Derenzo SE. Advances in positron tomography for oncology. Nucl Med Biol. 1996;23:659–667.
24. Frey EC, Li J, Tsui BMW. The importance of combined scatter and attenuation compensation in Tl-201 cardiac SPECT [abstract]. J Nucl Med. 1995;36(suppl):60P.
25. Knuuti MJ, Nuutila P, Ruotsalainen U, et al. Euglycemic hyperinsulinemic clamp and oral glucose load in stimulating myocardial glucose utilization during positron emission tomography. J Nucl Med. 1992;33:1255–1262.
26. Martin WH, Jones RC, Delbeke D, Sandler MP. A simplified intravenous glucose loading protocol for fluorine-18 fluorodeoxyglucose cardiac single-photon emission tomography. Eur J Nucl Med. 1997;24:1291–1297.
27. Kiat H, Berman DS, Maddahi J, et al. Late reversibility of tomographic myocardial thallium-201 defects: an accurate marker of myocardial viability. J Am Coll Cardiol. 1988;12:1456–1463.